Experiments in Fluids 21 (1996) 110–117 © Springer-Verlag 1996

Penetration length and diameter development of vortex rings generated by impacting water drops

F. Durst

Abstract The formation of water drops underneath nozzles was studied numerically to provide the basis for repeatable experimental drop formation. The drops detached from the nozzle and impacted on a free water surface forming vortex rings. Experimental results obtained through kinematographic studies of the penetration and growth of these vortex rings are presented. Variations of the penetration depth were measured, depending on the nozzle height above the water surface where the drops were formed. The experiments revealed that it is the *state of oscillation at impact* that defines the penetration length. Interesting variations of the vortex ring diameter with time were recorded. A good overall understanding of the behavior of the diameter variation was obtained when it was plotted as a function of the penetration depth.

1 Introduction

The author's interest in the penetration of vortex rings in water, that form on a free water surface by the impact of water drops, was gerenated by observations that vortices play an important role in the entrainment of oxygen into lakes during rainy periods. Measuring the oxygen concentration as a function of the distance of the free water surface revealed an oxygen penetration much faster than can be explained by turbulent diffusion. In addition, no gradient driven transport of oxygen was observed, usually requiring a clear maximum at the free water surface. A maximum of the oxygen concentration occurred in the author's observation in the deeper water regions. All this could only be explained by oxygen transport by discrete vortex rings, generated by falling rain drops. Qualitative studies showed that the water droplets, impacting on the free water surface of a lake, were saturated with oxygen and penetrated 10–20 cm deep, owing to the motion of the vortices they form. Various penetration depths were found and could be correlated with the diameter of the drop, and differences in depth seemed to be explainable with the state of drop oscillation, at the time the drop impacted on the free water surface.

The above qualitative observations led to an experimental study of the author using the equipment shown in Fig. 1. This consisted of a drop-generating nozzle, manufactured out of bronze and located at a heigth h above the free water surface of a container with dimensions $L_C = 120$ cm $\times$ $W_C =$ 40 cm $\times$ $H_C = 45$ cm and a water height of 40 cm. Two BOLEX cameras were employed to obtain kinematographic records of the locations and diameters of the vortex rings as a function of time after impact. One camera recorded the vortex ring of one experiment from the side of the water container and the other camera from the bottom, utilizing a 45° reflection prism located at the bottom of the water container. Taking 1000 pictures per second with the BOLEX cameras permitted the recording of the vortex ring diameter and the penetration length, respectively. Interesting results could be deduced from the records regarding the time variation of the vortex ring diameter and also the variation of the penetration depth with time. The resultant information is reported in the present paper.

To carry out vortex formation experiments with the equipment in Fig. 1 required some precautions. Initial experiments showed that highly repeatable vortex ring formation occurred only when very clean water, free of detergents, was employed. The room air in the laboratory also had to be filtered to avoid fast contamination of the free water surface. After one day of experiments, the water in the glass container had to be changed and filtering of the employed tap water was needed to yield the required cleanliness for repeatable vortex formations. Only with such precautions could the experimental results be obtained which are summarized in this paper.

To record photographically the vortex rings, the water for the generation of the drops was colored with $KMnO_4$. The concentration of $KMnO_4$ was chosen to be as small as possible to just provide the contrast for photographically recording the drop generated vortices. Using the $KMnO_4$-tracer reduced the surface tension of the water to about 51×10^{-3} N/m but this value remained stable during the experiments.

It was decided to publish this paper in the light of a recent paper by Peck and Sigurdson (1995) on the same topic. It is felt that the results given here complement their measurements. The present results provide a good insight into the physics of vortex flow and explain some phenomena observed on free water surfaces in nature.

Received: 4 July 1995/Accepted: 24 January 1996

F. Durst
Institute of Fluid Mechanics,
University of Erlangen-Nürnberg,
Cauerstr. 4, D-91058 Erlangen, Germany

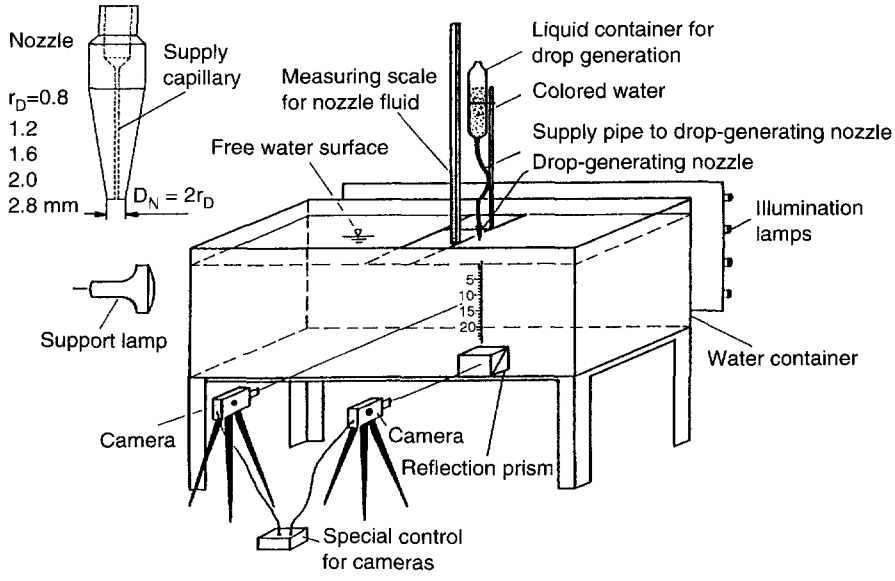

Fig. 1. Experimental set-up for investigations of vortex motion

2 Drop formation at nozzles

To yield reproducible drops for the present experiments required the drop formation underneath nozzles to be studied. First investigations were carried out numerically, following the theoretical study of quasi-static drop formation of Siemens (1954), Durst (1966) and Durst and Beer (1969). The quasi-static drop formation, was experimentally realized by a 40 mm long, small diameter supply capillary of 0.2 mm in diameter and by pressure controlling the water supply to the nozzle. The drop formation, the drop detachment, followed by drop oscillations were investigated by kinematographic records and are also reported below.

Figure 1 shows the nozzles that were employed to produce drops of different sizes. For this purpose the nozzle bottom diameter $2r_D = D_N$ was varied in the range given in Fig. 1. For all nozzle diameters given there, the droplet formation was studied experimentally and theoretically. As already mentioned, the theoretical studies could be based on the theory of static drop formation, using the following pressure relationship:

$$\frac{2\sigma}{R_0} - \rho_F g y = \sigma\left(\frac{1}{R_1}+\frac{1}{R_2}\right) - \rho_g g y$$

(with R_1 being the curvature in the y–r-plane) (1)

which can be rewritten as

$$\frac{1}{R_1}+\frac{1}{R_2} = \frac{2}{R_0} - \frac{g(\rho_F-\rho_g)}{\sigma} y \tag{2}$$

where R_1 and R_2 are the radii of curvature at a location (y, r) of the drop interface shown in Fig. 2, R_0 is the radius of curvature at $(y=0, r=0)$, g is the gravitational constant, σ is the surface tension, ρ_F is the liquid density and ρ_g is the density of the air surrounding the drop.

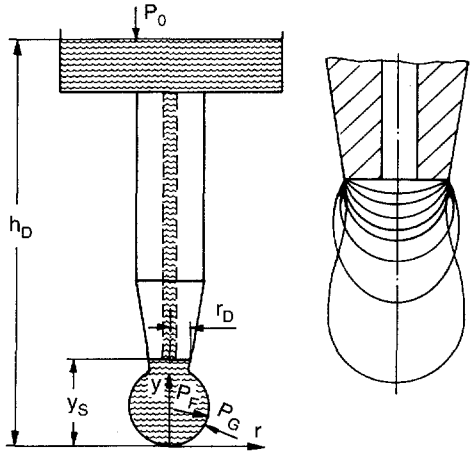

Fig. 2. Sketch of nozzle and fluid supply arrangement for studies of droplet formation beneath nozzles

Introducing the Laplace constant

$$a = \sqrt{\frac{2\sigma}{g(\rho_F-\rho_G)}} \tag{3}$$

permitted all geometric quantities to be normalized

$$\bar{r}=\frac{r}{a},\quad \bar{y}=\frac{y}{a} \quad \text{and} \quad \bar{R}_i=\frac{R_i}{a},\quad (i=0,1,2) \tag{4}$$

and the final non-dimensional differential equation read

$$\frac{1}{\bar{R}_1}+\frac{1}{\bar{R}_2} = 2\left(\frac{1}{\bar{R}_0}-\bar{y}\right) \tag{5}$$

Describing the radii $\bar{R}_1$ and $\bar{R}_2$ in terms of $\bar{y}$, $\bar{y}'$, $\bar{y}''$ and $\bar{r}$ yielded

$$\frac{\bar{y}''}{(1+\bar{y}'^2)^{3/2}} + \frac{\bar{y}'}{\bar{r}(1+\bar{y}'^2)^{1/2}} = 2\left(\frac{1}{R_0}-\bar{y}\right) \tag{6}$$

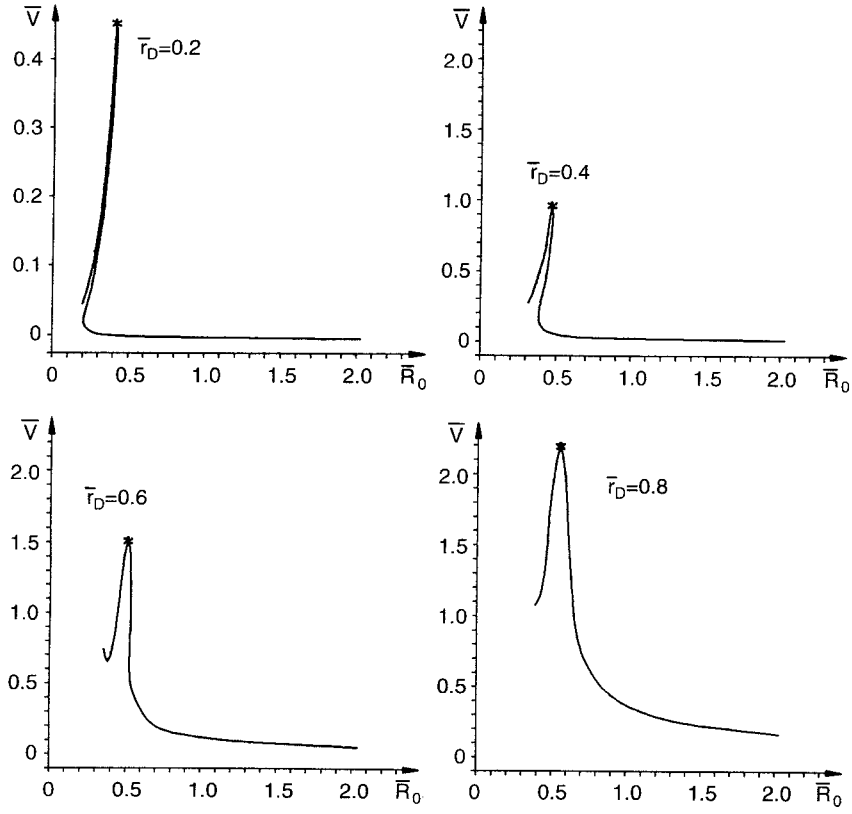

Fig. 3. Drop volume $\bar{V}_D$ as a function of bottom radius $\bar{R}_0$ of the drop

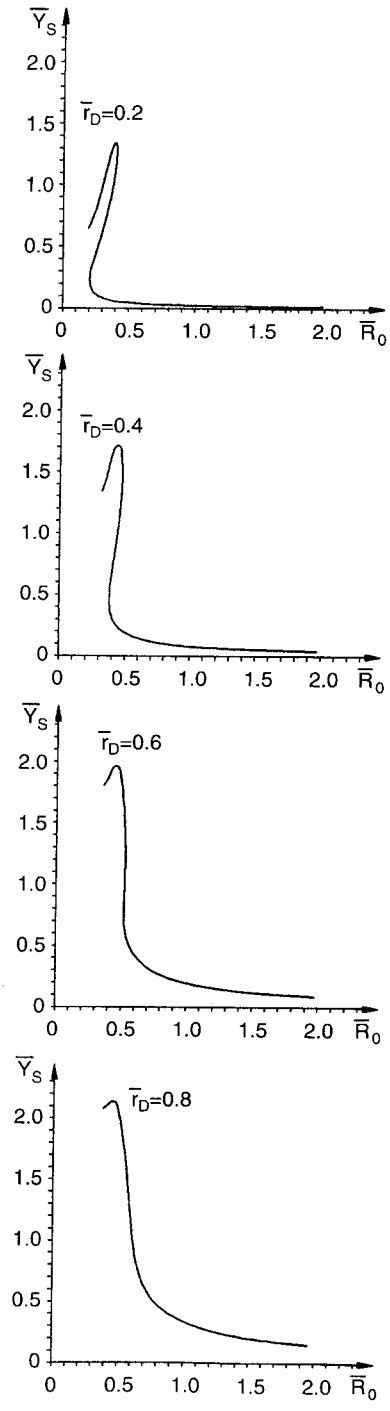

Fig. 4. Variation of distance of lowest point of drop interface from nozzle

Using this differential equation permitted the drop development at the nozzle to be computed using the following "starting and developing conditions" for the drop:

- The drops form at the bottom surface and the base area always occupies the nozzle surface with diameter $2r_D$.
- The start of the drop is any drop interface with $\bar{R}_{0,1} \geqslant 10.0$.
- The liquid flow through the center capillary is slow and always downwards to yield

$$\bar{V}_D(\bar{R}_{0,i+1}) > \bar{V}_D(\bar{R}_{0,i})$$

i.e. the droplet volume always grows with time.
- The drop detaches when the drop volume $\bar{V}_D$ reaches its first maximum.

Under these conditions, the drop developed as shown in Fig. 2 for $\bar{r}_D = 0.4$. The computed volume variation with R_0 is given in Fig. 3 (where $\bar{V}_D$ is the normalized volume of the drop from the surface at $\bar{y} = 0$ downwards). The maxima in this figure are the points of detachment of the drop. The above stated continuous liquid supply to the drop, however small it will be in practice, will ensure a repetition of drop formation which is physically defined.

The computed variations of $\bar{y}_s$, i.e. the distance of the lowest point of the drop surface, where the surface curvature is $\bar{R}_0$ are shown in Fig. 4 and the variation of the normalized pressure:

$$\bar{\Delta p}_D = \frac{[p_{F,D} - P_0 - \rho_L g h_D]}{\sqrt{2\sigma g(\rho_F - \rho_G)}} = \frac{1}{\bar{R}_0} - \bar{y}_0 \qquad (7)$$

$P_{F,D}$ = fluid pressure at nozzle level $\bar{y} = 0$, $\bar{\Delta p}_D$ = normalized pressure variation at nozzle level $\bar{y} = 0$; P_0 = atmospheric pressures, h_D = height of liquid above $\bar{y} = 0$ in Fig. 5. Taking $\bar{V} = \bar{V}_D$ as the free variable allows the quantities $\bar{y}$ and $\bar{\Delta p}_D$ to be plotted as functions of $\bar{V}$, as shown in Fig. 6 for $\bar{y}_s(\bar{V})$.

With the computed information on the drop formation, it became clear that a high repeatability of size and state of detachement of the drops could only be achieved, if the drop formation is controlled to be quasi static. For this purpose

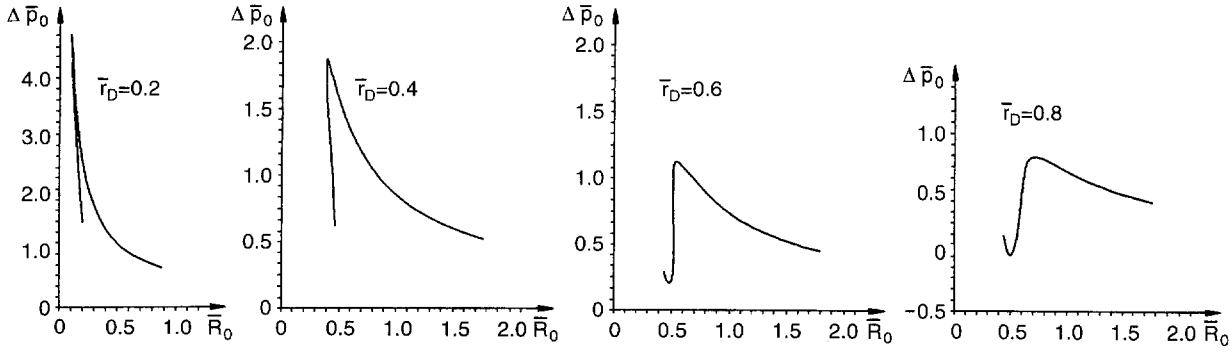

Fig. 5. Computed normalized pressure difference as a function of drop interface radius at the lowest point

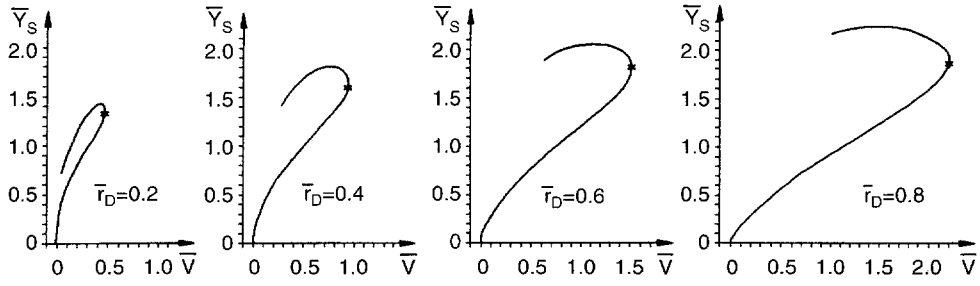

Fig. 6. Distance of the lowest point from the nozzle as a function of drop volume

a nozzle was constructed with a small, centrally located supply capillary of small diameter. This diameter was chosen to be $d=0.2$ mm and a capillary length of $l=40$ mm was found to help the drop formation to be very close to the computations given above. Hence, the numerical results given above helped to set up the experimental conditions for the experiments described in Sect. 1 and to obtain the results of Sect. 5.

Careful observations showed that the detachement of the drop from the downward facing nozzle, yielded an increase of the drop volume beyond the predicted maximum value shown in Fig. 3. This has also been reported by Siemens (1954), Durst (1966) and Durst and Beer (1969). Since it was the aim of the present study to yield highly repeatable drop sizes and not to know their volume at the time of detachment, no further investigations of the drop volumes were performed.

The studies of the time of drop formation were extended to the time after the drop detachment. Utilizing the kinematic records allowed the drop detachment to be studied, followed by oscillations of the falling drops. The general observations are sketched in Fig. 7. The actual drop volume was computed from photographic records of the kind sketched in Fig. 7.

The above described numerical investigations of the drop formation underneath nozzles helped to carry out the studies on the vortex formation by drops interacting with a free water surface. Approximate information on the nozzle diameter $D_N=2r_d$ could be computed by knowing the Laplace constant a. Furthermore, the nozzle height could be found out for which the drops started to interact with a free water surface prior to drop detachment. All experiments described below could therefore be performed with a sound knowledge on how the vortex generating drops formed underneath the employed

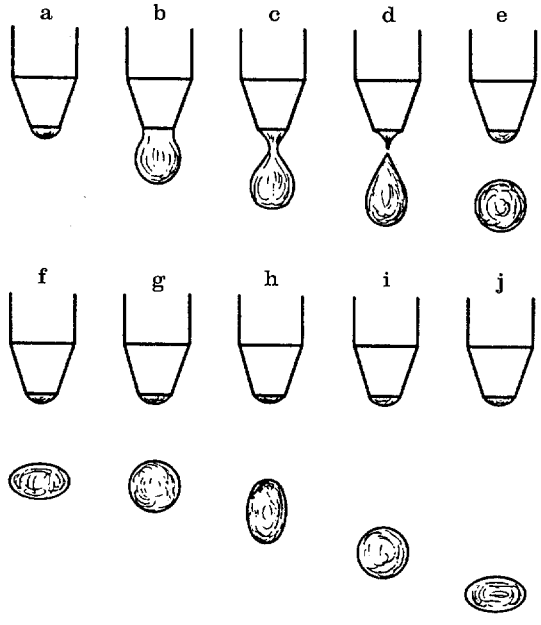

Fig. 7a–j. Sketch of drop formation, drop detachment and drop oscillations

nozzles and what properties they had when interfered with a free water surface.

5 Vortex formation and penetration depth

The initial investigations, after the study of repeatable drop formation, concentrated on the investigations of vortex

formation by drops impacting on the free water surface. It was found that the formation of the vortex rings depended on the "state of oscillation" of the drop on impact. This is indicated in Fig. 8, which shows the maximum penetration depth L_{max} of the vortex ring as a function of the nozzle height H above the water surface for the nozzle radius $r_D = 1.6$ mm. L was measured from kinematographic records, as the distance from the free water surface to the centre of the vortex ring at any downstream location, as seen by the BOLEX camera recording the side view of the vortices. L_{max} was the distance when the vortex ring practically came to a standstill.

It could be seen that the initial phase of vortex formation took place at a height where the drop detachment did not result in a free-falling drop. The drop was still attached to the drop-generating nozzle, interfered with the free interface and the liquid in the "still forming drop" was introduced, through the free water surface, into the water container, forming a downward-penetrating vortex ring. The penetration depth of the vortex ring showed, in this phase, an increase with height above the water surface of the drop-generating nozzle until a first maximum was reached. Thereafter the penetration depth decreased again and it was deduced from the kinematic records that this was due to the increase in the downward momentum of the drop showing detachment effects in its upper part when the lower part had already interacted with the free water surface, see lower left sketch of Fig. 8. The additional momentum gained by the drop due to the increased water height is not favorable for vortex ring formation, see also Chapman and Critchlow (1967). This resulted in a less perfect vortex ring, with a decreased capability to penetrate downwards.

After the first minimum of the penetration depth had been reached, an increase of L_{max} was recorded that could be allocated to the first "upward mode of oscillation" of the impacting drop. As the upper right sketch of Fig. 8 shows, the second maximum of the penetration depth occured when the drop oscillation was upward, taking away some of the downward momentum of the impacting drop. Similarly, the second minimum of penetration depth was caused by the "first downward mode of oscillation" on impact of the drop, see lower right sketch of Fig. 8. The further maxima and minima in Fig. 8 can be explained in the same way.

The above described variations of penetration depth as a function of nozzle height could be repeated and good agreement was achieved from one day to the other. However, the temperature in the water had to be controlled in order to make sure that roughly the same surface tensions existed in the different experiments. All experiments were performed within 46×10^{-3} N/m $\leqslant \sigma \leqslant 53 \times 10^{-3}$ N/m. To avoid thermal effects to influence the experimental results, the drop forming liquid was taken from the container to be at the same temperature. Lab and water temperature were kept at roughly the same value of about 18°C.

In order to demonstrate that the penetration depth characteristics in Fig. 8, given for $r_D = 1.6$ mm, hold for various drop sizes, the described experiments were repeated for the other nozzle diameters given in Fig. 8. The results are summarized in Fig. 9a–d. The same general behavior of the penetration depth with various nozzle heights is observed and the explanations given for the results in Fig. 8 for the cause of the maxima and minima of the penentration depth were found for each of the drop-generating nozzles employed in these experiments.

6 Variation of diameter of vortex rings

The quantitative evaluation of the kinematic records of the vortex motion inside the water tank yielded additional information, e.g. on diameter variations with time, as sketched in Fig. 10. Time was measured from the first touch of the water

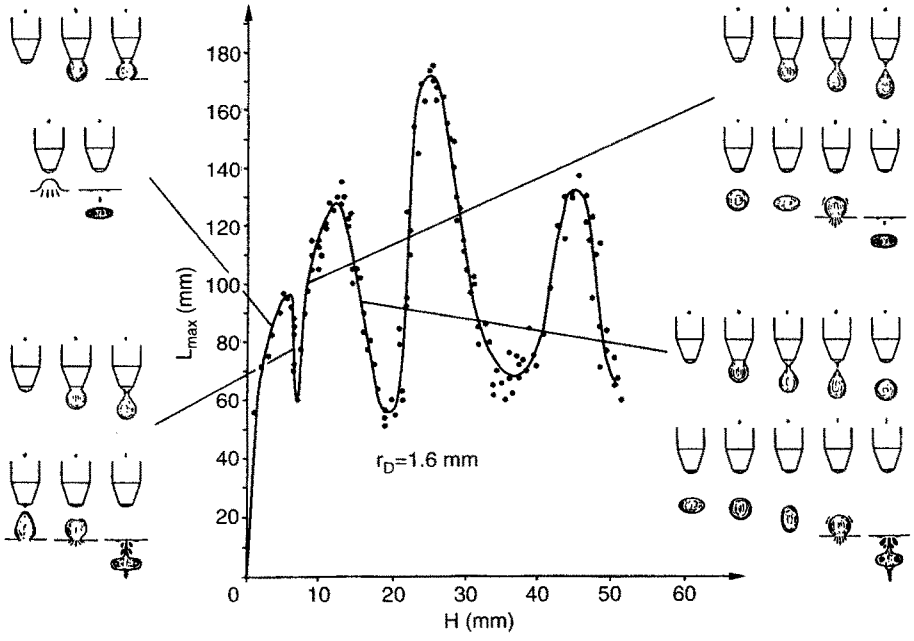

Fig. 8. Penetration depth as a function of nozzle height for nozzle radious $r_D = 1.6$ mm

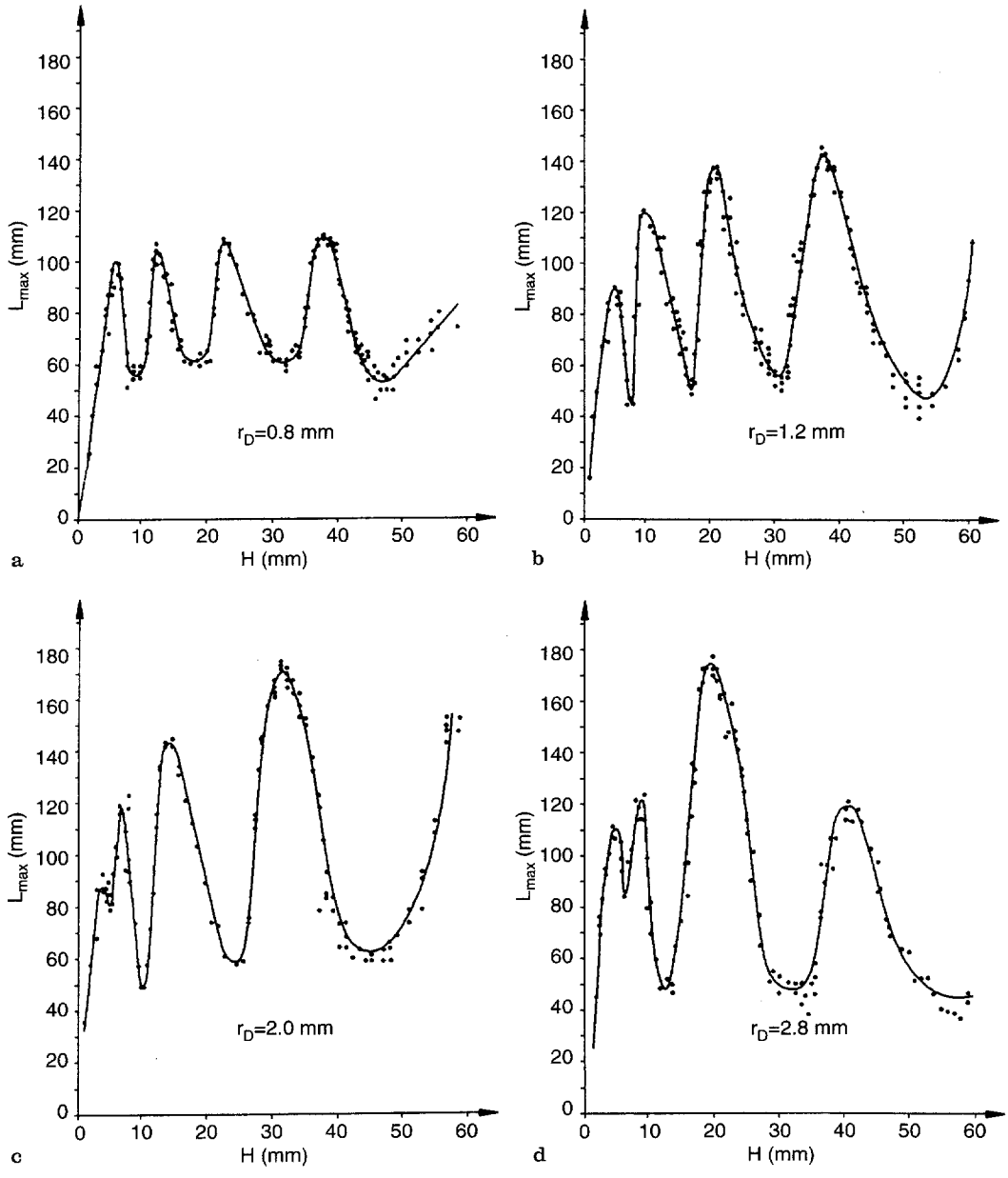

Fig. 9a–d. Penetration depth of vortex rings as a function of nozzle height for different nozzle diameters **a** $r_D = 0.8$ mm; **b** $r_D = 1.2$ mm; **c** $r_D = 2.0$ mm; **d** $r_D = 2.8$ mm

drop with the free surface and time pulses recorded on the kinematographic records were used to record $D(t)$ and $L(t)$. This information was stored in tables and used to obtain an insight into the vortex formation, the vortex penetration and the diameter growth with time.

It can be seen from Fig. 10 that the investigated vortex ring, for a large penetration depth, consisted of three major regions of motion. In the first region the vortex ring formed, which is characterized by a time period of nearly constant diameter D, followed by a time interval of very stable vortex motion (laminar region) where the diameter increased proportionalily to $t^{1/2}$. Some time later, a readily observable growth of flow disturbances took place in the experiment that caused the initial vortex ring to disintegrate. However, the disintegration resulted in the formation of a new vortex ring that showed an increase in diameter proportional to $t^{1/3}$. Figure 10 shows clearly the above mentioned three regions of *vortex formation* and of *laminar vortex motion*, followed by the *vortex disintegration* and the formation of a new vortex ring with a different flow behavior than for the initially formed ring.

Repeating the diameter studies for rings of smaller penetration depth revealed the general behavior shown in Fig. 10. This diameter variation with time shows basically the same general regions, but the vortex ring instabilities occurred earlier on the $t^{1/2}$ branch of the $D(t)$ development diagram. This is shown in Fig. 11a–c. The shorter the penetration length of the vortices was, the earlier the disintegration occured in time.

Since the information on $L(t)$ (penetration depth as a function of time) was also available, it was possible to represent the vortex ring diameter variation as a function of the

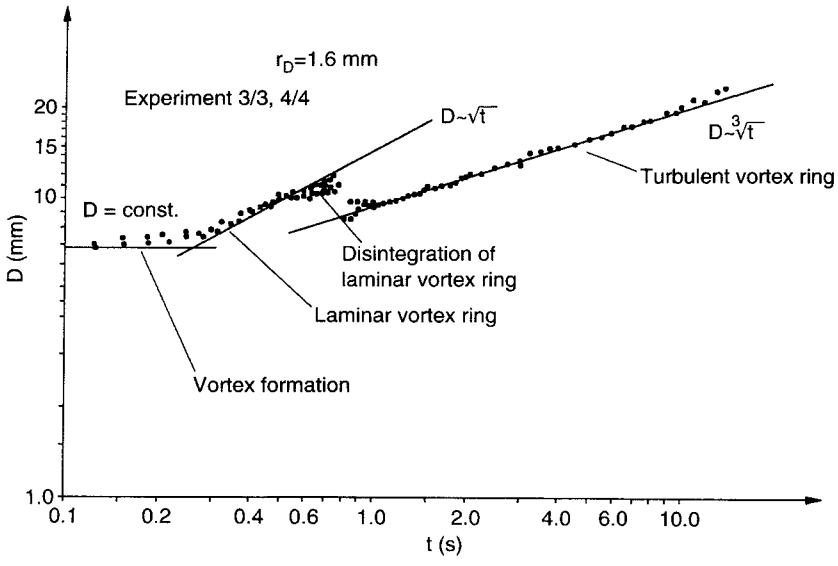

Fig. 10. Diameter of vortex rings a function of time after an impact. Vortex ring with $L_{max} \approx 170$ mm

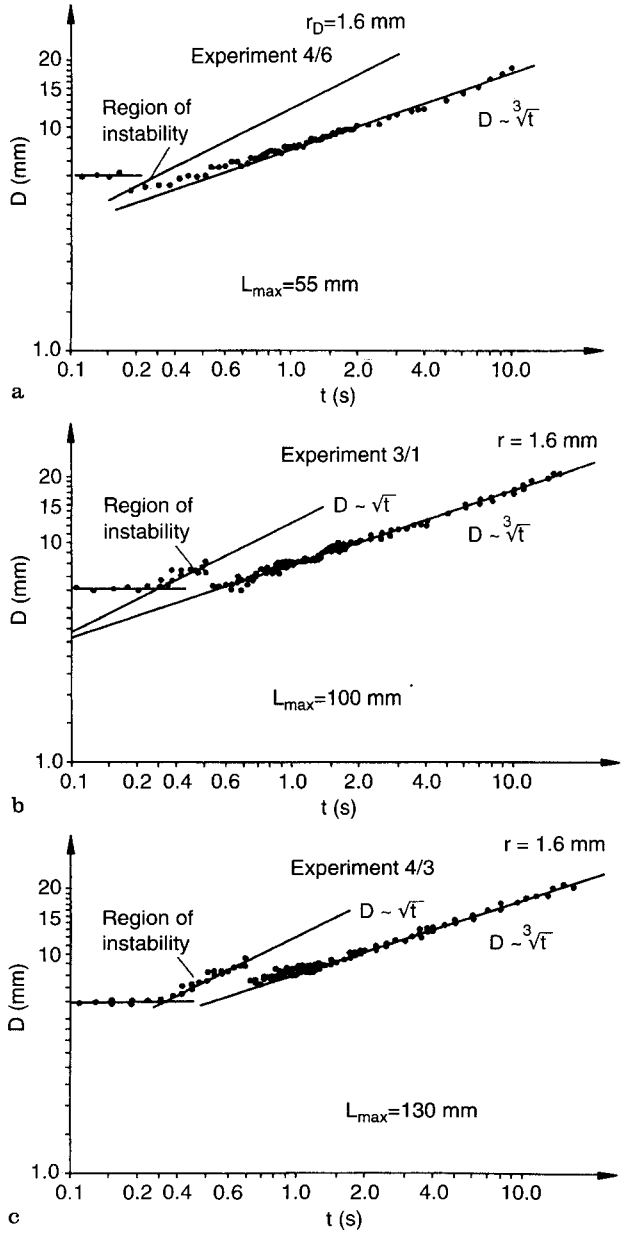

penetration depth. This resulted in Fig. 12, which clearly provides the data in a form which permits the formation of vortex rings and their motion to be described in general terms. The region of vortex ring formation clearly shows a region D = constant, followed by a transition region out of which the stable "laminar vortex section" emerges. At the end of this region, flow instabilities grow to such an extent that the rings disintegrate. The results show that vortex rings with large penetration depth disintegrate later than those characterized by lower penetration depths. The observed disintegration consisted of complete "loss of shape" of the laminar vortex ring followed by an observable reformation of a new vortex ring. After the instability has caused a disintegration, a new vortex ring forms which has his own D–L characteristics, as shown in Fig. 12.

7
Conclusions and final remarks

It is worth noting that other publications have dealt with the vortex ring formation and vortex ring motion stated in this paper and in the work of Peck and Sigurdson (1995). Some of the relevant literature has been quoted by Peck and Sigurdson, but additional papers should be mentioned here, e.g. by Kutter (1916), Krutzsch (1939) and Durst and Fuchs (1974). Utilizing the information available in the literature and the data in this paper yields a good insight into the properties of vortex rings generated at impact on a free water surface.

The present experiments revealed:

– Contamination of the free liquid surface and the liquid used to form the drops is the major cause of loss of repeatability of vortex formation and vortex penetration. Good temperature control is also needed for carefully carried out experiments. Vibrations of the equipment also need to be avoided to yield a high degree of repeatability in the experiments.

Fig. 11a–c. Variation of vortex ring diameter with time for vortex rings with different penetration depths

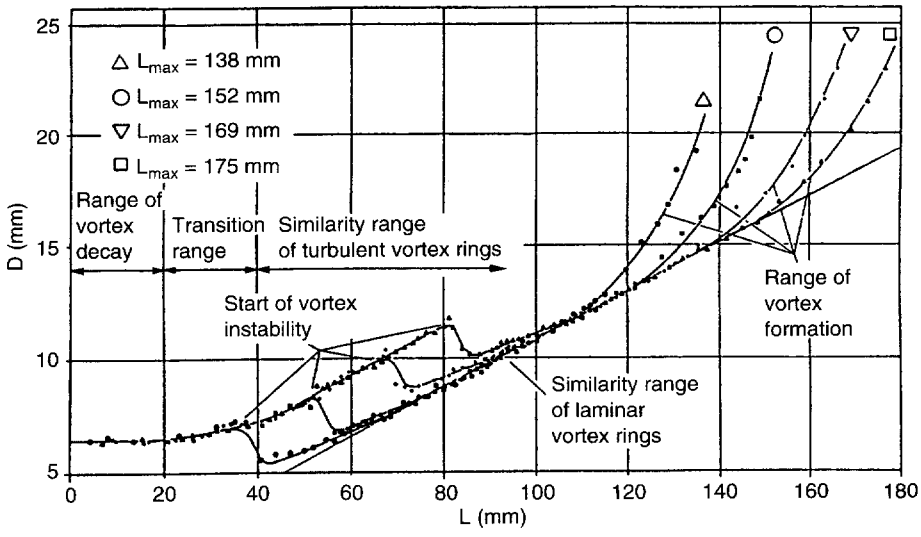

Fig. 12. Vortex ring diameter as a function of penetration depth. The diagram shows results for vortex rings with various penetration depth

– When a falling drop impacts on the free interface, there seems to be a short time lapse between impact and vortex ring formation. This seems to support the hypothesis of Chapman and Critschlow (1967) that the energy used to form the vortex ring results from the surface energy of the falling drop. Too much additional kinetic energy yields more unstable drops.

– The present experiments also support the observations of Chapman and Critchlow (1967) that the penetration depth of the vortex rings has a maximum when the drop has a spherical shape on impact and undergoes an oscillating motion that reduces its horizontal diameter and increases its vertical diameter. However, these observations are in disagreement with the findings of Kutter (1916), who did not observe vortex rings with maximum penetration depth for this state of oscillation.

– The present investigations allowed an insight into the physics of vortex formation by impacting water drops. The region of vortex formation is followed by a transitional region before the drop penetrates with a diameter variations proportional to $t^{1/2}$, the region of laminar vortex motion. This region is ended by the growth of instabilities, leading to disintegration of the vortex ring.

– The above mentioned disintegration of the vortex ring resulted in the reformation of a new ring which showed a different diameter – time behavior: it was found that the diameter grows with $t^{1/3}$ and the observation suggested the existence of turbulent vortex motion.

– When the diameter is plotted against penetration depth, the development region, regions of D proportional to $t^{1/2}$ and D proportional to $t^{1/3}$ clearly result in regions of vortex development, laminar vortex motion and turbulent vortices. Rings with the largest penetration depths develop their instability caused disintegration at a later stage.

– The remaining tracer liquid on the free water surface showed a circular shape when the vortex ring had a long penetration depth. For rings with short penetration depths, the traces on the free water surface showed wrinkles such as those obtained by Krutzsch (1939).

Finally, it should be mentioned that *some of the vortex rings* showed two phases of transition. The initial phase of the vortex ring showed the same formation and transitional properties as all the other rings. However, when the growth of instabilities disintegrated the vortex ring, a formation process started, followed by a second transition. This resulted in final vortex rings that showed a growth in diameter proportional to $t^{1/4}$. The cause of this second transition was not examined in closer detail, because it was felt that kinematographic studies alone are insufficient to obtain a deeper insight into the observed double transition phenomena. Advanced optical measuring techniques should be employed for further studies and also refined theoretical treatments are needed in order to deepen the insight into the penetration and diameter development of vortex rings generated by impacting water drops.

References

Chapman DS; Critchlow PR (1967) Formation of vortex rings from falling drops. J Fluid Mech 29:

Durst F (1966) Beitrag zur Bildung von Gasblasen an Düsen durch Gasdispersion in Flüssigkeiten, Diplomarbeit. Inst. Thermodynamik der Luft- und Raumfahrt, Universtät Stuttgart

Durst F; Beer H (1969) Blasenbildung an Düsen bei Gasdispersionen in Flüssigkeiten. Chem Ing Techn 41: 1000–1006

Durst F; Fuchs W (1974) Die Bildung von Wirbelringen durch fallende Tropfen und die Dynamik der Wirbelringfortbewegung. SFB 80/ET/23

Krutzsch Ch (1939) Über eine experimentell beobachtete Erscheinung an Wirbelringen bei ihrer translatorischen Bewegung in wirklichen Flüssigkeiten. Ann Phys Ser 5: 35

Kutter V (1916) Die Anwendung on Wirbelringen zur Bestimmung von Oberflächenspannungen. Physikalische Zeitschrift 23: 573–579

Peck B; Sigurdson L (1995) The vortex ring velocity resulting from an impacting water drop. Exp Fluids 18: 351–357

Siemens W (1954) Gasblasen in Düsenplatten, Teil I. Chem Ing Techn 26: 479–496